

Nano Research

September · 2021

Volume 14 · Number 9

Congratulations to Professor Dongyuan Zhao and Professor John A. Rogers on winning the 2020 Nano Research Award

Flagship Review Flexible organic solar cells for biomedical devices

Functional photonic structures for external interaction with flexible/wearable devices

Optoelectronic sensing of biophysical and biochemical signals based on photon recycling of a micro-LED



TSINGHUA
UNIVERSITY PRESS



Springer



Project for Enhancing International
Impact of China STM Journals

Optoelectronic sensing of biophysical and biochemical signals based on photon recycling of a micro-LED

He Ding¹, Guoqing Lv¹, Zhao Shi², Dali Cheng², Yang Xie², Yunxiang Huang³, Lan Yin³, Jian Yang¹, Yongtian Wang¹, and Xing Sheng² (✉)

¹ Beijing Engineering Research Center of Mixed Reality and Advanced Display, School of Optics and Photonics, Beijing Institute of Technology, Beijing 100081, China

² Department of Electronic Engineering, Beijing National Research Center for Information Science and Technology, Center for Flexible Electronics Technology, Tsinghua University, Beijing 100084, China

³ School of Materials Science and Engineering, Tsinghua University, Beijing 100084, China

© Tsinghua University Press and Springer-Verlag GmbH Germany, part of Springer Nature 2020

Received: 6 September 2020 / **Revised:** 19 November 2020 / **Accepted:** 21 November 2020

ABSTRACT

Conventional bioelectrical sensors and systems integrate multiple power harvesting, signal amplification and data transmission components for wireless biological signal detection. This paper reports the real-time biophysical and biochemical activities can be optically captured using a microscale light-emitting diode (micro-LED), eliminating the need for complicated sensing circuit. Such a thin-film diode based device simultaneously absorbs and emits photons, enabling wireless power harvesting and signal transmission. Additionally, owing to its strong photon-recycling effects, the micro-LED's photoluminescence (PL) emission exhibits a superlinear dependence on the external conductance. Taking advantage of these unique mechanisms, instantaneous biophysical signals including galvanic skin response, pressure and temperature, and biochemical signals like ascorbic acid concentration, can be optically monitored, and it demonstrates that such an optoelectronic sensing technique outperforms a traditional tethered, electrically based sensing circuit, in terms of its footprint, accuracy and sensitivity. This presented optoelectronic sensing approach could establish promising routes to advanced biological sensors.

KEYWORDS

photon recycling, photoluminescence, microscale light-emitting diodes (micro-LEDs), optoelectronics, biosensors

1 Introduction

Epidermal sensing systems based on advanced electronic and photonic materials and devices have gained significant interest in the past decade, owing to their versatile capabilities in monitoring biophysical (electrophysiology, temperature, pressure, etc.) and biochemical (oxygen, glucose, ions, etc.) activities with direct clinical relevance [1–4]. To realize remote, non-invasive, precise and continuous operation, various strategies utilizing microwave, optical, and ultrasound signals have been developed for wireless energy harvesting and signal transmission [5–9]. Conventional skin-mounted sensors, or bioelectronic sensors in general, still require sophisticated circuits with multiple device components, including at least a power supply, a signal amplifier and a data transmitter [10]. Alternatively, it is known that a semiconductor photodiode can serve as an energy generator (via the photovoltaic effect) and a light emitter (via the radiative recombination of carriers) [11]. Moreover, for a diode with high electron-to-photon and photon-to-electron conversion efficiencies, its photoluminescence (PL) can be leveraged by manipulating its photon-recycling effects based on varied electrical signals like voltage, current and resistance [12–16]. In other words, this implied that such a mechanism could provide an unusual way for probing biological signals.

In this paper, we demonstrated that the bioelectronic

activities can be optically monitored by simply using a thin-film, microscale light-emitting diode (micro-LED), with a footprint of about 100 μm (Fig. 1(a)). Such a micro-LED can simultaneously work as an energy absorber, a signal amplifier and an optical transmitter. The conductance dependent photon-recycling effect alters the micro-LED's luminescence under optical excitation. With its electrodes attached to the human skin, its optical signals can directly reflect the real-time skin resistance, or galvanic skin response (GSR) variations, with performance comparable to a commercial GSR sensing circuit module. In addition, we demonstrated that such an optoelectronic sensing mechanism is capable to achieve temperature or pressure detection when integrated within corresponding resistive sensors, as well as the monitoring of chemical substances like ascorbic acid. These promising characteristics of this introduced concept would provide a novel optical solution to realize the integrated and wireless biosensing.

2 Results and discussion

Figure 1(a) shows photographs of the indium gallium phosphide (InGaP) based red-emitting micro-LED attached on the human finger. The thin-film, freestanding InGaP micro-LED has a lateral dimension of $\sim 200 \mu\text{m} \times 150 \mu\text{m}$ and a thickness of $\sim 5.6 \mu\text{m}$, fabricated by epitaxial growth, lithographic etching,

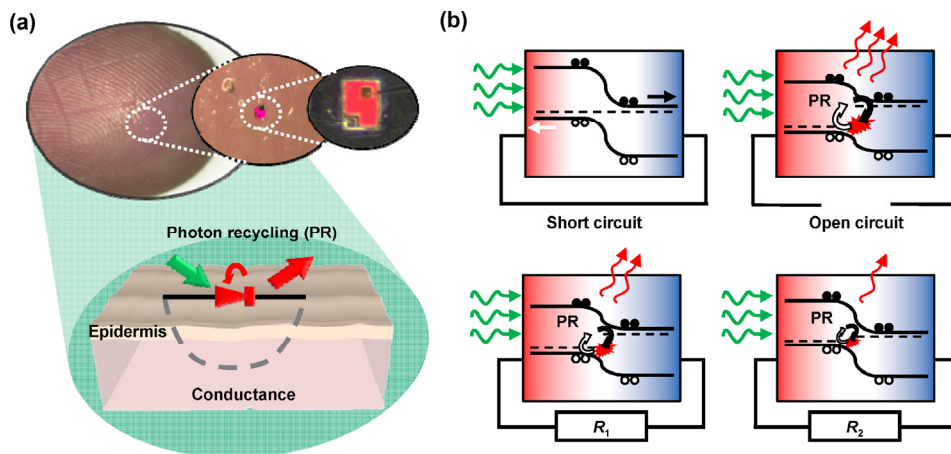


Figure 1 (a) Images and schematic illustrations of a thin-film, red-emitting micro-LED attached onto the human skin for wireless, optoelectronic sensing of the biophysical and biochemical signals based on its conductance dependent photon-recycling (PR) effect. The LED has lateral dimensions of 200 μm × 150 μm and a thickness of 5.6 μm. (b) The operational principle of the sensor, showing that the diode's PL intensity is dependent on its load resistances in different working conditions: short-circuit, open-circuit, and connected to different resistances ($R_1 > R_2$). Black and white dots indicate photogenerated free electrons and holes, and red, blue and white regions represent the p-type, n-type and depletion regions of the diode, respectively.

metal deposition, removal of the sacrificial layer and transfer printing (more details see the methods in the Electronic Supplementary Material (ESM)) [17]. For circuit-free operation, no current injection is provided through external power supplies like a battery. Instead, the micro-LED is optically illuminated with a green laser source, and its red PL emission can be captured through a 560 nm long-pass filter. Schematically illustrated in Fig. 1(b), its operational principle as a wireless GSR sensor can be understood based on the modeling of a simplified photodiode under optical excitation. In the short-circuit condition, most of the photogenerated carriers flow into the external circuit and recombine non-radiatively. At the open-circuit condition, on the contrary, the carriers recombine within the junction via photon recycling, creating a strong PL if the diode is made by III–V semiconductors with high external luminescence efficiencies (η_{ext}) [18–21]. In other words, the load resistance R alters the diode's built-in potential, thereby modulating its PL emission (PL intensity increases with R). In detail, the relationship between the diode's PL intensity and the loaded skin resistance R can be described by (see details in the ESM)

$$R = \frac{kT \ln \left(\frac{q n_{\text{photons}}}{J_{\text{th}} \eta_m} \right)}{q \left(J_{\text{ph}} + J_{\text{th}} - \frac{q n_{\text{photons}}}{\eta_m \eta_{\text{ext}}} \right) S} \quad (1)$$

where J_{ph} is the photogenerated current derived from the excitation light power density, J_{th} is the absorbed thermal radiation from the environment, S is the active surface area of the device, n_{photon} is the number of the captured emissive photons directly related to the PL intensity and the coupling efficiency of the microscope setup (η_m). It can be seen that an exponential relation between the PL emission and the resistance is obtained due to the diode characteristics, providing an effective amplification mechanism for GSR sensing.

Figures 2(a) and 2(b) present the details about the InGaP micro-LED structure, with more information provided in Table S1 in the ESM. We evaluated its GSR sensing capability by connecting it with different load resistances (Fig. 2(c)). Under the green light excitation (peaked at ~ 545 nm) with fixed power, the micro-LED's PL emission increases with the increased resistance values and reaches the maximum at the open-circuit condition (Fig. 2(d)). We further measured the

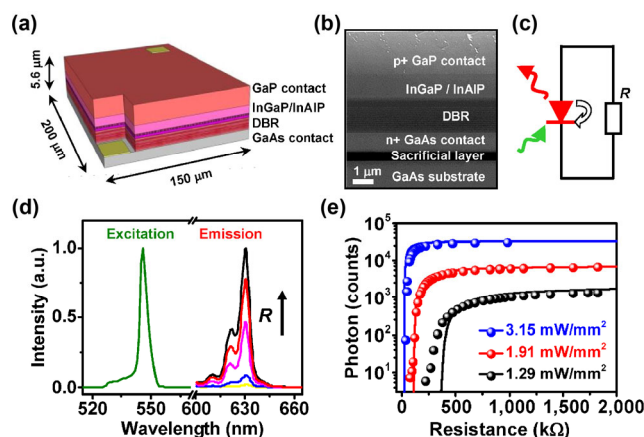


Figure 2 (a) Schematic diagram and (b) cross-sectional scanning electron microscopy (SEM) image of the micro-LED structure, including a GaP window/contact layer, InGaP/InAlP active layers, a distributed Bragg reflector (DBR) layer, and a GaAs contact layer. An $\text{Al}_{0.95}\text{Ga}_{0.05}\text{As}$ based sacrificial layer is between the active device and the GaAs substrate for subsequent etching to create freestanding thin-film devices. (c) Circuit model of the optoelectronic resistive sensing based on PR effects. (d) Measured spectra of the excitation source (green light) and PL emissions of the micro-LED connected with different resistors, showing increased PL intensities with resistance (from top to bottom: open-circuit, 650, 280, 145 and 120 kΩ). (e) Calculated (lines) and the measured (dots) PL intensity as a function of the load resistance under excitation light with different power densities (3.15 mW/mm² for blue, 1.91 mW/mm² for red and 1.29 mW/mm² for black lines and dots).

integrated emission intensity (unit: counts/μm²/ms) as a function of the resistance at various excitation power, using a fluorescence microscope equipped with a complementary metal oxide semiconductor (CMOS) camera (more details see the methods in the ESM). The results are plotted in Fig. 2(e), in comparison with the calculations based on Eq. (1). The measured PL intensity firstly increases exponentially with the resistance and then saturates when approaching the open-circuit condition, which is in accordance with the theoretical predictions. In addition, there is a trade-off between the resistance sensitivity and the detection limit of the measurement setup (~ 5–10 counts/μm²/ms). As shown in Refs. [22, 23] and subsequent experiments, the GSR levels for the human body normally lie within 100–500 kΩ, which are dependent on human conditions (health states, emotions, etc.) as well as the

environment (temperature, humidity, etc.). An excitation power of $\sim 1.91 \text{ mW/mm}^2$ is selected for actual GSR measurement involving human subjects, in which the skin is considered safe at such an excitation power density [24].

Figure 3 demonstrates the optically measured GSR results of a human subject. The InGaP micro-LED is connected between two different fingers using hydrogel-based wet electrodes (Fig. 3(a) and more details are shown in Fig. S3 in the ESM). When a phasic activity (e.g., an action of deep breath) is performed, the skin resistance drops in response to the stimulus [25], leading to decreased PL intensity compared to the basal condition (Fig. 3(b)). Real-time optical signals are collected in a certain time frame (up to 1,000 s), in direct comparison with electrically measured GSR results simultaneously recorded based on a commercial circuit module (Fig. 3(c) and Movies ESM1 and ESM2), in which the gray regions represent discrete deep breath actions and the blank regions represent resting state, respectively. Optical and electrical measurements exhibit an excellent quantitative agreement, showing a determination coefficient of 98.82% when fitting with the theoretical predictions (Fig. 3(d)). In this experiment, the measured GSR range is 120–240 k Ω ; however, resistance variations in other ranges can also be captured by optimizing the intensity of the excitation light (see Fig. 2(e)). Furthermore, the normalized variation of photon signals (I/I_0) is about 4 times larger than electrically measured GSR, demonstrating an inherent capability for amplification associated with the photon-recycling mechanism in the diode. The fluctuation of the measured PL signals is pertinent to various noise sources, which determine the device's sensitivity. As shown in Fig. S4 in the ESM, the temporal variation of the micro-LED's PL intensity is recorded when connecting to a constant resistance of 200 k Ω . The noise power spectra lie close to the noise limit of the CMOS camera, suggesting that the micro-LED introduces negligible instability to the optical sensing system. In accordance with the equivalent

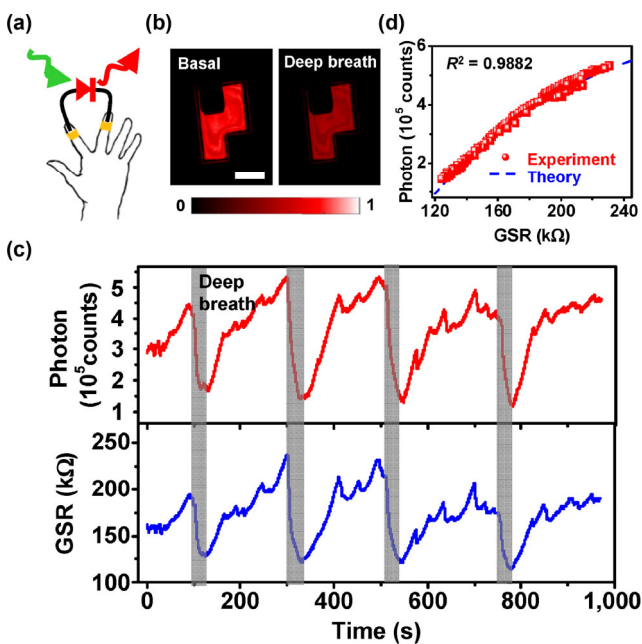


Figure 3 (a) Schematic illustration of the optoelectronic sensing of the GSR. (b) Microscopic images of the micro-LED's PL emission, showing different PL intensities under basal and deep breath conditions of a subject. (c) Simultaneously measured optical signals (top, red) and the electronic signals captured by a commercial GSR sensor (bottom, blue), as a function of time. Gray regions represent discrete deep breath actions of the tested subject, resulting in lower resistance of the epidermis. (d) Measured PL intensity versus GSR, in comparison with the fitting model.

relation, a resolution of $1.1 \text{ k}\Omega/\text{Hz}^{1/2}$ is obtained under this circumstance, by converting the dominant shot noise to the resistance noise. Furthermore, it should be noted that the optical noise is also dependent on the excitation power, which can be further optimized to the trade-off between the signal-to-noise ratio and the GSR sensitivity.

Owing to its unique optoelectronic sensing mechanism, the micro-LED can also be incorporated with other resistance-dependent transducers to monitor other physical and chemical signals [26]. As two vital physiological parameters for human, temperature and pressure are measured in-hospital diagnosis and home care as the standard procedure [27]. These signals can also be detected using our proposed optoelectronic sensing method, as shown in Fig. 4. The micro-LED is in a serial connection with a thermistor (Fig. 4(a)) or a piezoresistor (Fig. 4(c)), both of which are commercially available devices. In Fig. 4(b), the thermistor's resistance decreases as temperature increases. When it is connected to the optically excited micro-LED, its temperature-dependent resistance variance is optically presented as the change of the micro-LED's PL intensity. Based on the noise analysis in Fig. S4 in the ESM, the system's sensitivity is determined to be $\sim 1.2 \text{ }^\circ\text{C}$, on par with a commercial infrared thermometer, in which the accuracy is often affected by the surface emissivity of objects [28]. Similarly, optoelectronic sensing of pressure can be accomplished when the micro-LED is connected with a piezoresistor (Fig. 4(d)). Both of the experimental results are in good accordance with the theoretical models, of which the details are presented in the ESM. In this regard, such an optoelectronic based detection mechanism shows great potentials when applying in numerous biophysical sensing scenarios.

On the other hand, chemical detection of various biomolecules has attracted tremendous attention recently, offering new opportunities with promises for biological sensing, health monitoring and clinical diagnostics [29]. As one of the standard detection techniques, the electrochemical based method has been widely utilized for biochemical sensing, because of its high sensitivity, simplicity, and low cost [29, 30]. Along with many chemical substances excreted from sweat, ascorbic acid (AA) is a cofactor in many enzymatic reactions in the

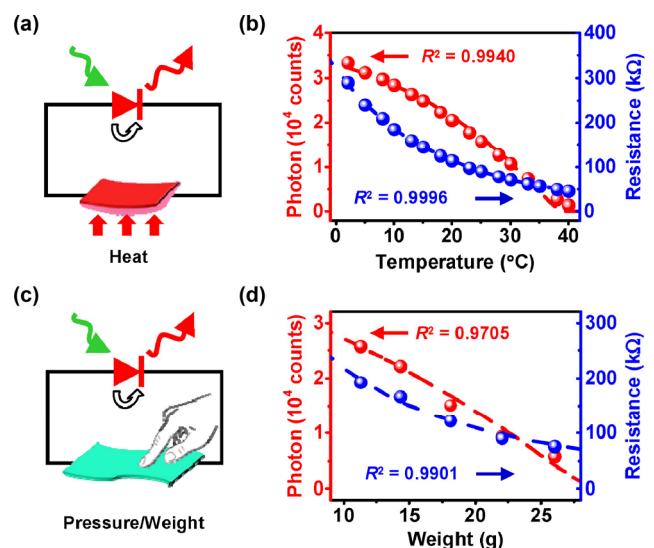


Figure 4 (a) and (c) Schematic illustrations of the micro-LED based optoelectronic sensing of temperature and pressure. Here the optically excited micro-LED is serially connected to a thermistor (a) or a piezoresistor (c). (b) and (d) Measured (dots) and theoretical (lines) of PL intensity (red) as a function of the temperature or pressure, in comparison with the resistive responses of the sensors (blue).

human body that mediate a variety of essential biological functions [31, 32]. Here we showed that the micro-LED based optoelectronic sensing can also be employed as an alternative and wireless scheme for electrochemical detection, as shown in Fig. 5. Schematically illustrated in Fig. 5(a), the two terminals of the micro-LED are connected with platinum electrodes that are immersed in the phosphate-buffered saline (PBS) solution (0.01 M, pH = 5) with varied AA concentrations. Under optical illumination, the anode of the micro-LED supplies a forward bias, oxidizing AA to dehydroascorbic acid (DHA). Such an electrochemical reaction consumes electrical currents in the circuit, decreases photogenerated carriers that can otherwise recombine within the micro-LED, followed by a decline of PL intensity (see the ESM for detailed theoretical analysis). With increased AA concentrations, the dynamic response of the micro-LED's PL intensity is captured and presented in Fig. 5(b). When comparing with simultaneously measured current within the circuit (Fig. S5 in the ESM), it is clearly seen that increased electrochemical reaction currents lead to decreased PL intensities. Figure 5(c) further compares the result of adding PBS with AA with that of adding pure PBS as a control, confirming that the current variation is directly associated with the electrochemical reaction. As plotted in Fig. 5(d), the micro-LED's PL intensity is linearly dependent on the concentration of AA within the range of 0–170 μM , covering the normal AA concentration range in the sweat (34–114 μM) and other biofluids (for example, 28–63 μM in blood) [33, 34]. The detection sensitivity is determined to be ~ 16 photons/ μM . These preliminary results clearly validate the device's optoelectrochemical sensing capability, and also exhibit the ability to sense different redox reactions with functionally modified electrodes for practical applications. In the future research, microscale and nanoscale LEDs can also be designed to realize wireless and remote biochemical detection with a high resolution and a high selectivity, based on such an optoelectronic mechanism [35].

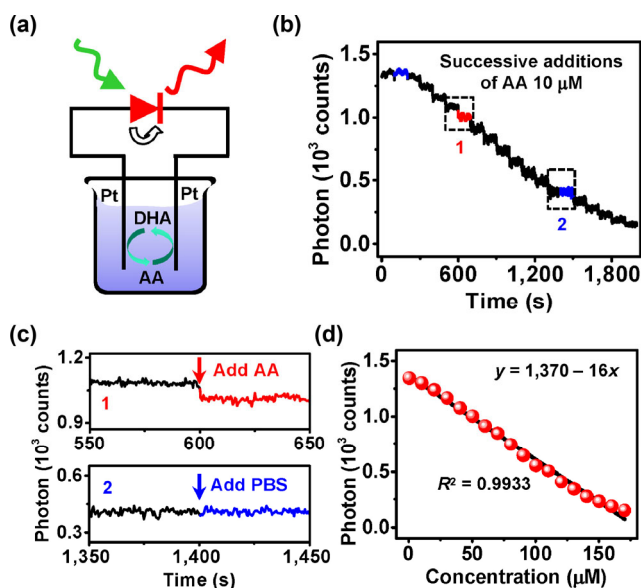


Figure 5 (a) Schematic illustration of the micro-LED based optoelectronic sensing of the AA. Here the optically excited micro-LED is serially connected to two Pt electrodes that are inserted into PBS solutions (0.01 M, pH = 5). (b) Opto-chronoamperometric response for successive additions of 10 μM AA in the PBS, with a stirring rate of 200 rpm/min. (c) The representative temporal PL responses of the micro-LED for the experimental group with the addition of the 10 μM AA, and the control group with the PBS. (d) Calibration curve of the PL intensity as a function of the AA concentrations.

3 Conclusion

To summarize, here we demonstrate that the biophysical and biochemical signals, e.g., electrodermal activities, temperature, pressure and ascorbic acid, can be optically monitored in an all-in-one concept, simply by utilizing a micro-LED with the conductance-dependent PL emissions. The high photon-to-electron and electron-to-photon conversion efficiencies of III–V semiconductors enable the device to harness the power and emit sensing signals purely optically. In addition, the photon-recycling process in the diode junction endows the device to optically respond to the conductance variation with high sensitivity. It is envisioned that such a device approach can be further employed to detect many other biophysical and biochemical signals *in vitro* and *in vivo*, with high sensitivity and specificity. Future directions would also involve the formation of devices arrays in the micro and nano scale, to realize bio-signal mapping at the high spatial and temporal resolution, for example, for cultured cell imaging. For *in vivo* applications in the future, miniaturized systems incorporating optical excitation and detection capabilities can be explored for portable measurements. Collectively, we believe that this optoelectronic strategy can offer a novel paradigm for next-generation biosensors in general.

4 Experimental sections

4.1 Device fabrication

The detailed InGaP based thin-film red micro-LED structure is shown in Table S1 in the ESM, which was grown on a GaAs substrate by using the metal-organic chemical vapor deposition (MOCVD) method. A 500 nm thick SiO_2 as the hard mask was deposited via plasma-enhanced chemical vapor deposition (PECVD) method. The wafer was lithographically patterned with desired geometry and following etching of SiO_2 in buffered oxide etchant (BOE), GaP in $\text{KOH}/\text{K}_3[\text{Fe}(\text{CN})_6]/\text{H}_2\text{O}$ (1:4:15, by weight), InAlP/MQWs/InAlP/DBR in $\text{HCl}:\text{H}_3\text{PO}_4$ solution (1:1, by volume), GaAs/AlGaAs/GaAs layer in $\text{H}_3\text{PO}_4:\text{H}_2\text{O}:\text{H}_2\text{O}$ solution (3:1:25, by volume). The Ge/Ni/Au and Cr/Au served as Ohmic electrodes for n-type and p-type GaAs contact layers, respectively. Freestanding thin-film micro-LED devices were achieved by complete removal of the sacrificial layer ($\text{Al}_{0.95}\text{Ga}_{0.05}\text{As}$) in diluted hydrofluoric acid (HF) based solution (HF:water = 1:10 by volume, with few drops of ethanol). With the help of patterned poly(dimethylsiloxane) (PDMS) stamps, released devices were picked up and transferred to various carrier substrates (glass, plastics, skin, etc.) with a coated thin-film adhesive layer.

4.2 Device characterization

Current–voltage characteristics of the micro-LED device were recorded using a Keithley 2400 source meter, to provide the parameters for the fitting models. The illuminated micro-LED device was imaged with an Olympus IX53 microscope equipped with a Xenon arc lamp, in which the excitation light and the emission light passed through a set of fluorescence filter combinations (EX AT540/25x, BS AT565DC, EM AT605/55m, Chroma Tech. Corp.). The PL density of the illuminated micro-LED was collected by the Andor Zyla 4.2Plus CMOS camera with the exposure time of 5 ms. An area of $\sim 20 \mu\text{m}^2$ (100 pixels) was chosen to avoid the interference fringes on the surface of the micro-LED device from the epoxy coating.

4.3 GSR measurements

Four independent hydrogel-based wet Ag/AgCl electrodes were

applied on the fingers of a human subject as shown in Fig. S3(a) in the ESM. Two of the electrodes were connected to the micro-LED PL sensing system (Fig. S3(b) in the ESM), and the other two were connected to a commercial GSR circuit module (DLCK365, Techtronic) (Fig. S3(c) in the ESM). The excitation power was $\sim 1.91 \text{ mW/mm}^2$.

4.4 Optoelectrochemical measurements

The anode and cathode of the micro-LED were connected with two platinum electrodes (diameter $\sim 0.3 \text{ mm}$), which were immersed in the solution at a depth of $\sim 2 \text{ cm}$. Droplets of $50 \mu\text{L}$ 10 mM AA in PBS solutions (0.01 M , $\text{pH} = 5$ diluted with hydrochloric acid) were successively added into the 50 mL PBS solution (0.01 M , $\text{pH} = 5$), with a stirring rate of 200 rpm/min . The PL intensity of the micro-LED and the current in the circuit were simultaneously measured (Fig. S7 in the ESM). The excitation power was $\sim 1.29 \text{ mW/mm}^2$.

Acknowledgements

Funding: the National Natural Science Foundation of China (NSFC) (No. 61874064); Beijing Institute of Technology Research Fund Program for Young Scholars; Beijing Innovation Center for Future Chips, Tsinghua University; Beijing National Research Center for Information Science and Technology (No. BNR2019ZS01005). The authors acknowledge characterization work supported by Beijing Institute of Technology Analysis & Testing Center. We also thank Nianzhen Du for the image design.

Electronic Supplementary Material: Supplementary material (detailed analytical calculation of photoluminescence intensities of the micro-LED connected with different loads by considering the photon-recycling effect) is available in the online version of this article at <https://doi.org/10.1007/s12274-020-3254-2>.

References

- [1] Kim, D. H.; Lu, N. S.; Ma, R.; Kim, Y. S.; Kim, R. H.; Wang, S. D.; Wu, J.; Won, S. M.; Tao, H.; Islam, A. et al. Epidermal electronics. *Science* **2011**, *333*, 838–843.
- [2] Gao, W.; Emaminejad, S.; Nyein, H. Y. Y.; Challa, S.; Chen, K.; Peck, A.; Fahad, H. M.; Ota, H.; Shiraki, H.; Kiriya, D. et al. Fully integrated wearable sensor arrays for multiplexed *in situ* perspiration analysis. *Nature* **2016**, *529*, 509–514.
- [3] Imani, S.; Bandodkar, A. J.; Mohan, A. M. V.; Kumar, R.; Yu, S. F.; Wang, J.; Mercier, P. P. A wearable chemical–electrophysiological hybrid biosensing system for real-time health and fitness monitoring. *Nat. Commun.* **2016**, *7*, 11650.
- [4] Kim, J.; Campbell, A. S.; de Ávila, B. E. F.; Wang, J. Wearable biosensors for healthcare monitoring. *Nat. Biotechnol.* **2019**, *37*, 389–406.
- [5] Chung, H. U.; Kim, B. H.; Lee, J. Y.; Lee, J.; Xie, Z. Q.; Ibler, E. M.; Lee, K.; Banks, A.; Jeong, J. Y.; Kim, J. et al. Binodal, wireless epidermal electronic systems with in-sensor analytics for neonatal intensive care. *Science* **2019**, *363*, eaau0780.
- [6] Reynolds, M. F.; Guimarães, M. H. D.; Gao, H.; Kang, K.; Cortese, A. J.; Ralph, D. C.; Park, J.; McEuen, P. L. MoS_2 pixel arrays for real-time photoluminescence imaging of redox molecules. *Sci. Adv.* **2019**, *5*, eaat9476.
- [7] Piech, D. K.; Johnson, B. C.; Shen, K.; Ghanbari, M. M.; Li, K. Y.; Neely, R. M.; Kay, J. E.; Carmena, J. M.; Maharbiz, M. M.; Muller, R. A wireless millimetre-scale implantable neural stimulator with ultrasonically powered bidirectional communication. *Nat. Biomed. Eng.* **2020**, *4*, 207–222.
- [8] Bariya, M.; Nyein, H. Y. Y.; Javey, A. Wearable sweat sensors. *Nat. Electron.* **2018**, *1*, 160–171.

- [9] Cortese, A. J.; Smart, C. L.; Wang, T. Y.; Reynolds, M. F.; Norris, S. L.; Ji, Y. X.; Lee, S.; Mok, A.; Wu, C. Y.; Xia, F. et al. Microscopic sensors using optical wireless integrated circuits. *Proc. Natl. Acad. Sci. USA* **2020**, *117*, 9173–9179.
- [10] Lou, Z.; Wang, L. L.; Jiang, K.; Wei, Z. M.; Shen, G. Z. Reviews of wearable healthcare systems: Materials, devices and system integration. *Mater. Sci. Eng. R Rep.* **2020**, *140*, 100523.
- [11] Neamen, D. A. *Semiconductor Physics and Devices*, 3rd ed.; McGraw-Hill: Boston, 2003.
- [12] Ding, H.; Hong, H.; Cheng, D. L.; Shi, Z.; Liu, K. H.; Sheng, X. Power- and spectral-dependent photon-recycling effects in a double-junction gallium arsenide photodiode. *ACS Photonics* **2019**, *6*, 59–65.
- [13] Sheng, X.; Yun, M. H.; Zhang, C.; Al-Okaily, A. M.; Masouraki, M.; Shen, L.; Wang, S. D.; Wilson, W. L.; Kim, J. Y.; Ferreira, P. et al. Device architectures for enhanced photon recycling in thin-film multijunction solar cells. *Adv. Energy Mater.* **2015**, *5*, 1400919.
- [14] Peng, M. Z.; Li, Z.; Liu, C. H.; Zheng, Q.; Shi, X. Q.; Song, M.; Zhang, Y.; Du, S. Y.; Zhai, J. Y.; Wang, Z. L. High-resolution dynamic pressure sensor array based on piezo-phototronic effect tuned photoluminescence imaging. *ACS Nano* **2015**, *9*, 3143–3150.
- [15] Stolterfoht, M.; Le Corre, V. M.; Feuerstein, M.; Caprioglio, P.; Koster, L. J. A.; Neher, D. Voltage-dependent photoluminescence and how it correlates with the fill factor and open-circuit voltage in perovskite solar cells. *ACS Energy Lett.* **2019**, *4*, 2887–2892.
- [16] Macka, M.; Piasecki, T.; Dasgupta, P. K. Light-emitting diodes for analytical chemistry. *Annu. Rev. Anal. Chem.* **2014**, *7*, 183–207.
- [17] Ding, H.; Lu, L. H.; Shi, Z.; Wang, D.; Li, L. Z.; Li, X. C.; Ren, Y. Q.; Liu, C. B.; Cheng, D. L.; Kim, H. et al. Microscale optoelectronic infrared-to-visible upconversion devices and their use as injectable light sources. *Proc. Natl. Acad. Sci. USA* **2018**, *115*, 6632–6637.
- [18] Marti, A.; Balenzategui, J. L.; Reyna, R. F. Photon recycling and Shockley's diode equation. *J. Appl. Phys.* **1997**, *82*, 4067–4075.
- [19] Miller, O. D.; Yablonovitch, E.; Kurtz, S. R. Strong internal and external luminescence as solar cells approach the Shockley–Queisser limit. *IEEE J. Photovolt.* **2012**, *2*, 303–311.
- [20] Tex, D. M.; Imaizumi, M.; Akiyama, H.; Kanemitsu, Y. Internal luminescence efficiencies in InGaP/GaAs/Ge triple-junction solar cells evaluated from photoluminescence through optical coupling between subcells. *Sci. Rep.* **2016**, *6*, 38297.
- [21] Su, Z. C.; Xu, S. J.; Wang, X. H.; Ning, J. Q.; Wang, R. X.; Lu, S. L.; Dong, J. R.; Yang, H. Effective photon recycling and super long lived minority carriers in GaInP/GaAs heterostructure solar cell: A time-resolved optical study. *IEEE J. Photovolt.* **2018**, *8*, 820–824.
- [22] Richter, C. P. Physiological factors involved in the electrical resistance of the skin. *Am. J. Physiol-Legacy Content* **1929**, *88*, 596–615.
- [23] Boucsein, W. *Electrodermal Activity*, 2nd ed.; Springer: New York, 2012.
- [24] Sliney, D. H.; Wolbarsht, M. *Safety with Lasers and other Optical Sources: A Comprehensive Handbook*; Springer: New York, 1980.
- [25] Frijda, N. H. *The Emotions*; Cambridge University Press: Cambridge, 1986.
- [26] Yang, Y. B.; Yang, X. D.; Tan, Y. N.; Yuan, Q. Recent progress in flexible and wearable bio-electronics based on nanomaterials. *Nano Res.* **2017**, *10*, 1560–1583.
- [27] Zhang, F. J.; Zang, Y. P.; Huang, D. Z.; Di, C. A.; Zhu, D. B. Flexible and self-powered temperature–pressure dual-parameter sensors using microstructure-frame-supported organic thermoelectric materials. *Nat. Commun.* **2015**, *6*, 8356.
- [28] Rogalski, A. Infrared detectors: An overview. *Infrared Phys. Technol.* **2002**, *43*, 187–210.
- [29] Emaminejad, S.; Gao, W.; Wu, E.; Davies, Z. A.; Yin Yin Nyein, H.; Challa, S.; Ryan, S. P.; Fahad, H. M.; Chen, K.; Shahpar, Z. et al. Autonomous sweat extraction and analysis applied to cystic fibrosis and glucose monitoring using a fully integrated wearable platform. *Proc. Natl. Acad. Sci. USA* **2017**, *114*, 4625–4630.
- [30] Liu, C. B.; Zhao, Y.; Cai, X.; Xie, Y.; Wang, T. Y.; Cheng, D. L.; Li, L. Z.; Li, R. F.; Deng, Y. P.; Ding, H. et al. A wireless, implantable optoelectrochemical probe for optogenetic stimulation and dopamine detection. *Microsyst. Nanoeng.* **2020**, *6*, 64.

- [31] Levine, M.; Conry-Cantilena, C.; Wang, Y.; Welch, R. W.; Washko, P. W.; Dhariwal, K. R.; Park, J. B.; Lazarev, A.; Graumlich, J. F.; King, J. et al. Vitamin C pharmacokinetics in healthy volunteers: Evidence for a recommended dietary allowance. *Proc. Natl. Acad. Sci. USA* **1996**, *93*, 3704–3709.
- [32] Zhang, X.; Cao, Y.; Yu, S.; Yang, F. C.; Xi, P. X. An electrochemical biosensor for ascorbic acid based on carbon-supported PDN in nanoparticles. *Biosens. Bioelectron.* **2013**, *44*, 183–190.
- [33] Dhara, K.; Debiprosad, R. M. Review on nanomaterials-enabled electrochemical sensors for ascorbic acid detection. *Anal. Biochem.* **2019**, *586*, 113415.
- [34] Bernstein, R. E. Excretion of vitamin C in sweat. *Nature* **1937**, *140*, 684–685.
- [35] Wang, Y. C.; Zhu, H. L.; Yang, H. R.; Argall, A. D.; Luan, L.; Xie, C.; Guo, L. Nano functional neural interfaces. *Nano Res.* **2018**, *11*, 5065–5106.

Optoelectronic sensing of biophysical and biochemical signals based on photon recycling of a micro-LED

He Ding¹, Guoqing Lv¹, Zhao Shi², Dali Cheng², Yang Xie², Yunxiang Huang³, Lan Yin³, Jian Yang¹, Yongtian Wang¹, and Xing Sheng² (✉)

¹ Beijing Engineering Research Center of Mixed Reality and Advanced Display, School of Optics and Photonics, Beijing Institute of Technology, Beijing 100081, China

² Department of Electronic Engineering, Beijing National Research Center for Information Science and Technology, Center for Flexible Electronics Technology, Tsinghua University, Beijing 100084, China

³ School of Materials Science and Engineering, Tsinghua University, Beijing 100084, China

Supporting information to <https://doi.org/10.1007/s12274-020-3254-2>

1 Photoluminescence (PL) intensity of the micro-LED connected with different resistances

When considering its photon-recycling effect, the InGaP micro-LED behaves simultaneously as a photovoltaic cell and an LED [1, 2]. Under this circumstance, the micro-LED could be an optically-powered red emitter to sense the resistance change of the external circuit (Figure S1). Under illumination, the output current density from the diode is equal to the difference between generated carriers and recombined carriers based on the detailed balance (DB) theory [1, 3].

$$J = J_{\text{generation}} - J_{\text{recombination}} = J_{\text{ph}} + J_{\text{th}} - J_{\text{rad}} - J_{\text{nrad}} \quad (\text{S1})$$

where J_{ph} is the photogenerated current density and derived from the incident photons (J_{inc}) as shown in equation (S2), J_{th} is the absorbed thermal radiation from the environment as shown in equation (S3), and the J_{rad} is the radiative current, and J_{nrad} is the non-radiative current. The excitation light at a wavelength of 540 nm is absorbed in the active layer (α is the absorption coefficient and z is the thickness of InGaP/AlInP layer), which is conformed to the Beer-Lambert Law [4]:

$$J_{\text{ph}} = J_{\text{inc}} \exp(-\alpha_{540} z) \quad (\text{S2})$$

The thermal radiative current density (J_{th}) is defined as:

$$J_{\text{th}} = \frac{2\pi(n^2 + 1)qkT}{h^3 c_1^2} E_g^2 \exp\left(-\frac{E_g}{kT}\right) \quad (\text{S3})$$

where h is Planck's constant, k is Boltzmann's constant, c_1 is the speed of light, T is the temperature, n is the refractive index and E_g is the bandgap of the InGaP.

As the external radiative efficiency (η_{ext}) is defined as:

$$\eta_{\text{ext}} = \frac{J_{\text{rad}}}{J_{\text{rad}} + J_{\text{nrad}}} \quad (\text{S4})$$

where η_{ext} is highly associated with the internal quantum efficiency (IQE) and the out of coupling efficiency, with the estimated value of 70% and 3.9%, respectively [5, 6].

The output current density (J) can be shorted to:

$$J = J_{\text{ph}} + J_{\text{th}} - J_{\text{rad}} / \eta_{\text{ext}} \quad (\text{S5})$$

The output current (I) can be shorted to:

$$I = (J_{\text{ph}} + J_{\text{th}} - J_{\text{rad}} / \eta_{\text{ext}}) S \quad (\text{S6})$$

So the output voltage (V) is equal to the output current pass through the resistor in the external circuit:

$$V = (J_{\text{ph}} + J_{\text{th}} - J_{\text{rad}} / \eta_{\text{ext}}) SR \quad (\text{S7})$$

where S is the size of the device (surface area) and the R is total resistance, including the resistance of the diode and the external circuit. Compared to the dry skin resistance in the range of the 100–500 k Ω [7, 8], the resistance of the diode is $\sim 110 \Omega$ (obtained by fitting the experimental current–voltage data as shown in Figure S5) can be neglected under this circumstance.

Meanwhile, the emitted photons related to the micro-LED radiative current density will be generated with the photovoltage, which the voltage across the diode is equal to the voltage applied for the circuit ($V_{\text{rad}} = V$):

$$\begin{aligned}
 J_{\text{rad}} &= J_{\text{th}} \exp\left(\frac{qV_{\text{rad}}}{kT}\right) \\
 &= J_{\text{th}} \exp\left(\frac{q\left(J_{\text{ph}} + J_{\text{th}} - J_{\text{rad}}/\eta_{\text{ext}}\right)SR}{kT}\right)
 \end{aligned} \tag{S8}$$

So the relation between the resistance in the circuit and PL intensity of the micro-LED can be transformed to:

$$R = \frac{kT \ln\left(\frac{J_{\text{rad}}}{J_{\text{th}}}\right)}{q\left(J_{\text{ph}} + J_{\text{th}} - J_{\text{rad}}/\eta_{\text{ext}}\right)S} \tag{S9}$$

As the PL photons are derived from the radiative current of the diode and captured with the microscope (objective lens 20×, numerical aperture 0.5):

$$n_{\text{Photons}} = \frac{J_{\text{rad}}}{q} \eta_{\text{m}} \tag{S10}$$

where n_{photon} is the number of the captured emissive photons and η_{m} is the coupling efficiency of the microscope setup (about 12.5%).

So the number of the measured PL photons versus the resistance in the external circuit can be further expressed as:

$$R = \frac{kT \ln\left(\frac{qn_{\text{Photons}}}{J_{\text{th}}\eta_{\text{m}}}\right)}{q\left(J_{\text{ph}} + J_{\text{th}} - \frac{qn_{\text{Photons}}}{\eta_{\text{m}}\eta_{\text{ext}}}\right)S} \tag{S11}$$

which is the Eq. (1) in the main text.

2 Photoluminescence (PL) intensity of the micro-LED connected with the resistance-dependent temperature or pressure sensors

As the photoexcited InGaP micro-LED is acted as both the power source and visible indicator thanks to the photon-recycling process, this novel sensing optoelectronic sensing concept could extend to other domains with the aid of the series-connected resistance-dependent sensor.

The negative temperature coefficient (NTC) thermistor (MF55 104F3950) is applied to realize the optoelectronic temperature sensing function. The resistance (R) of the NTC thermistor at the temperature (T) is:

$$R = R_0 \exp\left[B\left(\frac{1}{T} - \frac{1}{T_0}\right)\right] \tag{S12}$$

where $B = 4162$ K is a constant, $R_0 = 8.93 \times 10^4 \Omega$ at $T_0 = 298$ K, obtained from manufacturers datasheet. So PL photons versus the temperature can be expressed as:

$$R_0 \exp\left[B\left(\frac{1}{T} - \frac{1}{T_0}\right)\right] = \frac{kT \ln\left(\frac{qn_{\text{Photons}}}{J_{\text{th}}\eta_{\text{m}}}\right)}{q\left(J_{\text{ph}} + J_{\text{th}} - \frac{qn_{\text{Photons}}}{\eta_{\text{m}}\eta_{\text{ext}}}\right)S} \tag{S13}$$

The force sensing resistor (FSR) (IMS003-C10A) is passive elements that function as a variable resistor based on the piezoresistive sensing mechanism. As conductance is proportional to pressure, the resistance (R) of FSR versus the pressure or weight (W) can be expressed as:

$$R = \frac{1}{a + bW} + c \tag{S14}$$

where $a = 1.144 \times 10^{-6} \Omega^{-1}$, $b = 2.616 \times 10^{-7} (\text{g} \cdot \Omega)^{-1}$, and $c = -4.685 \times 10^4 \Omega$, which are obtained from the device datasheet.

So the number of PL photons versus the pressure or weight (W) can be expressed as:

$$\frac{1}{a + bW} + c = \frac{kT \ln\left(\frac{qn_{\text{Photons}}}{J_{\text{th}}\eta_{\text{m}}}\right)}{q\left(J_{\text{ph}} + J_{\text{th}} - \frac{qn_{\text{Photons}}}{\eta_{\text{m}}\eta_{\text{ext}}}\right)S} \tag{S15}$$

3 Photoluminescence (PL) intensity of the micro-LED relevant to electrochemical reactions

According to the Cottrell equation [9], the electrochemical current is defined as:

$$I_{EC} = \frac{zFAC\sqrt{D}}{\sqrt{\pi t}} = MC \quad (S16)$$

where I_{EC} is the electrochemical current, z is the number of electrons transferred in the reaction, F is the Faraday constant, A is the area of the electrode, t is time, C is the concentration of the reducible analyte, D is diffusion coefficient for species. When extracting data at the same time point after changing the concentration of the analyte, the current exhibits a linear response to the concentration with the coefficient of M .

The electrochemical current can be regarded as the output current (equation (S6)) in this optoelectrochemical sensing circuit.

$$I_{EC} = (J_{ph} + J_{th} - J_{rad} / \eta_{ext})S \quad (S17)$$

As the concentration of the electrolyte is linear related to the electrochemical current changes, the number of PL photons versus the concentration (C) can be expressed as:

$$(J_{ph} + J_{th} - J_{rad} / \eta_{ext})S = MC \quad (S18)$$

Then the equation (S18) can be simplified as:

$$J_{rad} = \eta_{ext}(J_{ph} + J_{th} - MC) \quad (S19)$$

References

- [1] Martí, A.; Balenzategui, J. L.; Reyna, R. F. Photon recycling and Shockley's diode equation. *J. Appl. Phys.* **1997**, *82*, 4067-4075.
- [2] Miller, O. D.; Yablonovitch, E.; Kurtz, S. R. Strong internal and external luminescence as solar cells approach the Shockley–Queisser limit. *IEEE J. Photovolt.* **2012**, *2*, 303-311.
- [3] Shockley, W.; Queisser, H. J. Detailed balance limit of efficiency of p-n junction solar cells. *Journal of Applied Physics* **1961**, *32*, 510-519.
- [4] Russian Journal of Electrochemistry Swinehart, D. F. The Beer-Lambert law. *J. Chem. Educ.* **1962**, *39*, 333.
- [5] Ganapati, V.; Steiner, M. A.; Yablonovitch, E. The voltage boost enabled by luminescence extraction in solar cells. In *2016 IEEE 43rd Photovoltaic Specialists Conference (PVSC)*, 2016, pp 3499-3501.
- [6] Tex, D. M.; Imaizumi, M.; Akiyama, H.; Kanemitsu, Y. Internal luminescence efficiencies in InGaP/GaAs/Ge triple-junction solar cells evaluated from photoluminescence through optical coupling between subcells. *Sci. Rep.* **2016**, *6*, 38297.
- [7] Richter, C. P. Physiological factors involved in the electrical resistance of the skin. *Am. J. Physiol.* **1929**, *88*, 596-615.
- [8] Boucsein, W. *Electrodermal activity*. Springer: 2012.
- [9] Allen, J. B.; Larry, R. F. *Electrochemical methods fundamentals and applications*. John Wiley & Sons: 2001.

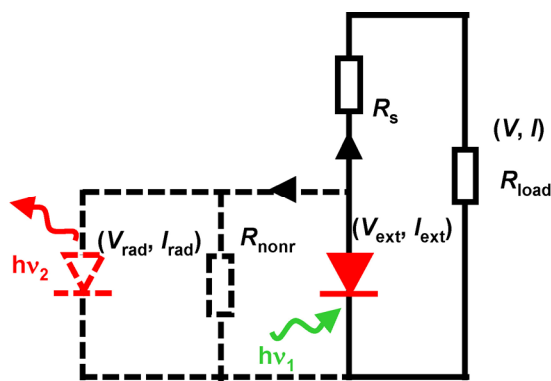


Figure S1 The equivalent circuit model to analyze the photon-recycling effect of the micro-LED connected to an external load resistance R_{load} .

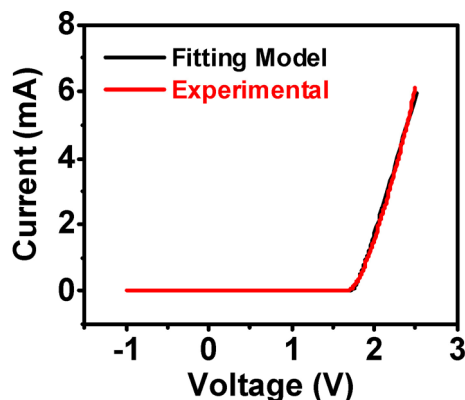


Figure S2 Measured current–voltage characteristics of the micro-LED, in comparison with the fitting results based on the model.

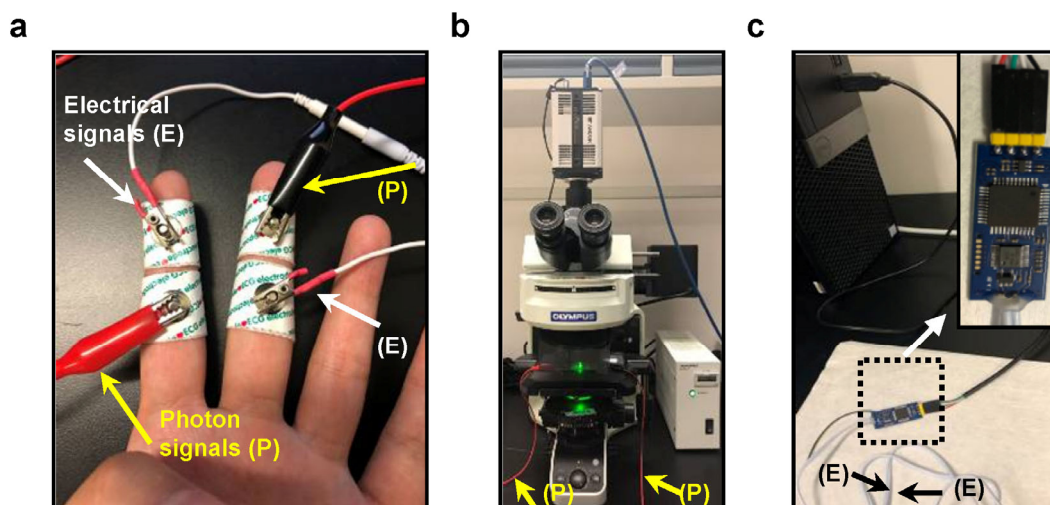


Figure S3 (a) Configuration for simultaneous optical and electrical collection of the GSR signals. Hydrogel based wet electrodes are applied on the fingers of a subject, which are linked to (b) a fluorescent microscope and (c) a commercial GSR sensing module for optical and electrical measurements, respectively.

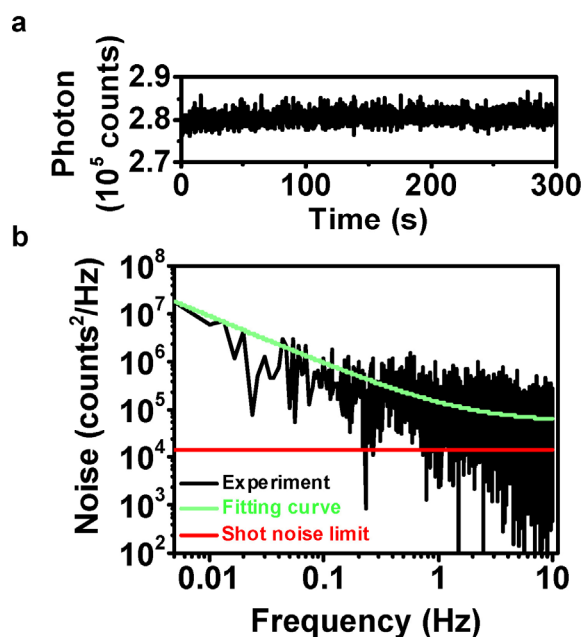


Figure S4 (a) The photon counts and (b) the corresponding power spectral density of the PL signals for the micro-LED connected with a 200 k Ω resistor under an excitation power of 1.91 mW/mm².

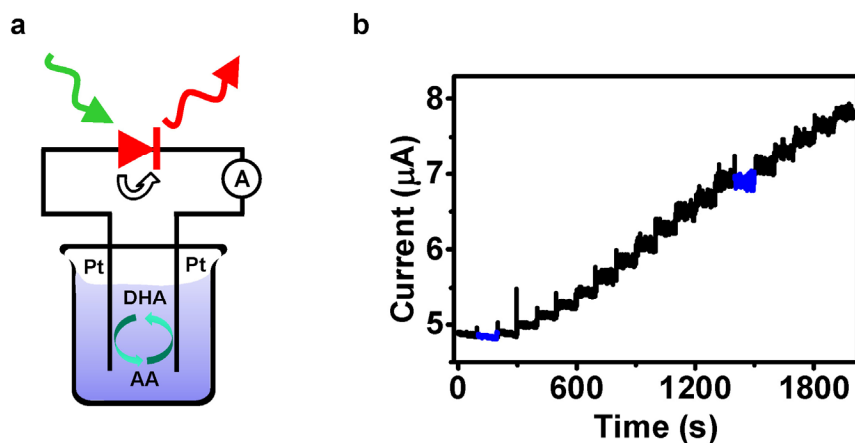


Figure S5 (a) Schematic illustration of electrochemical current measurement in the optoelectronic sensing experiment. (b) Chronoamperometric response for successive addition of 10 μ M AA in the PBS.

Table S1 Epitaxial structures of the InGaP red LED grown on the GaAs substrate.

| materials | thickness (nm) | doping (cm ⁻³) | dopant | |
|--|----------------|----------------------------|--------|---------------------|
| p++ GaP contact | 200 | 1e20 | C | } InGaP red LED |
| p+ GaP window | 2000 | 5e18 | Mg | |
| p InAlP | 800 | 1e18 | Mg | |
| InAlP / InGaP MQWs | 200 | - | - | |
| n InAlP | 200 | 8e17 | Si | |
| In _{0.5} Al _{0.5} P / In _{0.5} Al _{0.25} Ga _{0.25} P DBR 12 loops | 1200 | 3e18 | Si | — DBR |
| n+ GaAs contact | 1000 | 6e18 | Si | — ohmic contact |
| Al _{0.95} Ga _{0.05} As sacrificial | 500 | - | - | — sacrificial layer |
| GaAs substrate | - | - | - | |

Movie

Movie ESM1. Video showing: (left) the change of PL intensities of the micro-LED under the deep breath condition of a subject, (right) real-time recordings of photon and electrical signals, collected by a fluorescence microscope and a commercial GSR sensor, respectively.

Movie ESM2. Speeded up video (3× speed) of Movie ESM1.